Journal of Oceanography (2020) 76:389–400
https://doi.org/10.1007/s10872-020-00552-8

ORIGINAL ARTICLE

Spatial and temporal scales of sea surface salinity in the tropical Indian Ocean from SMOS, Aquarius and SMAP

Senliang Bao[1] · Huizan Wang[1] · Ren Zhang[1] · Hengqian Yan[1] · Jian Chen[2]

Received: 20 October 2019 / Revised: 19 May 2020 / Accepted: 22 May 2020 / Published online: 12 June 2020

Abstract
The spatial and temporal decorrelation scales of sea surface salinity (SSS) have been calculated in the tropical Indian ocean from the satellite measurements including Soil Moisture and Ocean Salinity (SMOS), Aquarius, Soil Moisture Active Salinity (SMAP), and the model output data for the period of 2011–2017. The differences in spatial and temporal scales from different products are discussed and the physical interpretations of the scales of SSS variability are analysed. The results show that, despite the differences in spatial and temporal resolution, there is good agreement between the spatial and temporal scales of SSS field among all products. Large zonal scales (> 2000 km) and temporal scales with strong anisotropy appear in the central of the equatorial Indian Ocean (8° S–15 °S). In addition, the large meridional decorrelation lengths (~ 800 km) and temporal scales with low anisotropy are found in the southern region of the Arabian Sea (0–12 °N) for all products. The decorrelation scales of SSS in these two areas are mainly caused by freshwater flux and salinity advection, respectively. Our results provide new insights into the controlling mechanisms of SSS variability in different regions.

Keywords Sea surface salinity · Decorrelation scales · Tropical Indian Ocean

1 Introduction

Salinity has been considered as a critically important parameter that influences the global water cycle, thermohaline circulation, and climate change (Ballabrera-Poy et al. 2002; de Boyer Montégut et al. 2007; Durack and Matear 2012; Li et al. 2016; Wang and Zhang 2012; Zhu et al. 2014). Therefore, salinity has been chosen as an essential climate variable (ECV) by the Global Climate Observing System (GCOS) (Belward et al. 2016). Despite the significance of salinity, the availability of in situ measurements (e.g., Argo floats, moored platforms, ship-based measurements) is inadequate in both space and time over recent decades (Bao et al. 2019). Fortunately, three satellite missions designed to measure sea surface salinity from space have been launched recently. The European Space Agency's (ESA) Soil Moisture and Ocean Salinity (SMOS) mission was launched in November 2009; Aquarius/SAC-D operated from 2011–2015, and the Soil Moisture Active Passive (SMAP) mission has operated since 2015. Satellite salinity data from these missions have allowed unprecedented monitoring of global distributions of SSS at mesoscale scales and the study of underlying relationships between SSS and both thermohaline circulation and climate change (Durand et al. 2013; Felton et al. 2015; Fournier et al. 2016; Hasson et al. 2018; Menezes et al. 2014; Nyadjro and Subrahmanyam, 2016; Yan et al. 2019).

Decorrelation scales of SSS, which are the typical size of the coherent variables features, can help with the understanding of spatial and temporal SSS variability and related processes that can affect SSS (Tzortzi et al. 2016). In addition, the information about decorrelation scales also helps in mapping irregularly sampled observations via objective analysis or optimal interpolation (OI), such as making gridded Level 3 (L3) satellite products from Level 2 (L2) data (Melnichenko et al. 2014), and SSS data assimilation (Mu et al. 2019). However, compared with other global variables such as sea surface temperature (SST) (Hosoda and Kawamura 2004; Meyers et al. 1991) and sea surface height (SSH) (Jacobs et al. 2001; Kuragano and Kamachi 2000), studies of the spatial and temporal scales of SSS are inadequate due to the limited coverage of in situ salinity measurements. Some

✉ Huizan Wang
wanghuizan@126.com

[1] College of Meteorology and Oceanography, National University of Defense and Technology, Deya Road, Changsha, China

[2] Beijing Institute of Applied Meteorology, Beijing, China

efforts have been made to estimate the scale of SSS variability using in situ data or model outputs (Delcroix et al. 2005; Martins et al. 2015). With the launch of the salinity satellites, Tzortzi et al (2016) estimated the spatial and temporal decorrelation scales of SSS in the Tropical Atlantic using SMOS and Aquarius 3-year (2012–2014) SSS data. Bingham and Lee (2017) used the Aquarius Version-4.0 data to quantify decorrelation scales of sea surface salinity (SSS) over the global ocean (60° S and 60° N) and discussed the relationship between SSS and surface freshwater flux.

The tropical Indian Ocean (TIO) plays a unique role in the global climate system. The Indian Ocean is rich in precipitation and it has the most typical monsoon climate of the global ocean. Owing to the significant monsoon and the existence of seasonal currents, SSS in the tropical Indian Ocean has strong seasonal and interannual variability modes (Grunseich et al. 2011; Momin et al. 2015). Many studies have mainly focused on the mechanism of SSS variability at different spatial and temporal scales (Rao, 2003; Subrahmanyam et al. 2011; Du and Zhang, 2015; Li et al. 2016) and its relationship with the Indian Ocean climate mode (Zhang et al. 2016, 2018). However, to the best of our knowledge, there are few related studies on the scales of SSS variability in the tropical Indian Ocean. The goal of this study was to expand on the work of Delcroix et al. (2005) and Bingham and Lee (2017) by providing more detailed characteristic spatial and temporal decorrelation scales in the tropical Indian Ocean using SSS observations from SMOS, Aquarius, and SMAP during the period 2010–2017 along with model outputs from the HYbrid Coordinate Ocean Model (HYCOM) and OGCM For the Earth Simulator (OFES). A distinctive feature of this study is the combination of long time series satellite SSS data from different missions with model outputs. In addition, we aimed to analyse the commonality of SSS decorrelation scales from different products and to provide physical interpretations of SSS scale variability.

This paper is organized as follows. Data and the method are presented in Sect. 2. Section 3 presents the results of the spatial and temporal scales. Finally, discussion and conclusion are presented in Sect. 4.

2 Data and method

Four up-to-date gridded L3 satellite products released are elected in the work, including SMOS BEC L3 data (abbreviated as SMOS BEC), SMOS CATDS CEC-LOCEAN L3 data (abbreviated as SMOS Catds), Aquarius V5.0 L3 data (abbreviated as Aquarius) and SMAP L3 SSS products (abbreviated as SMAP). The SMOS BEC data are obtained from debiased non-Bayesian BEC advanced global ocean products V1.0 provided by the Barcelona Expert Center (BEC) in Spain, which are generated from SMOS L1B TBs v620 using a new methodological approach to cope with land and RFI contamination (Olmedo et al. 2017). The 9-day running mean L3 maps with the spatial resolution of 0.25° × 0.25° are used here. Its time range is 1 January 2011 to 30 April 2017. The SMOS Catds data used in the study is the 9-day CEC-Locean L3 Debiased v3.0 maps at a spatial resolution of 0.25° × 0.25° developed by the Centre Aval de Traitement des Données SMOS (CATDS) in France, which reduced systematic errors and improved SSS natural variability varying spatially (Boutin et al. 2018). The time range of SMOS Catds is 1 January 2011 to 31 August 2017. The Aquarius L3 7-day Rain-flagged standard Mapped Image V5.0 products at 1° × 1° are used here, which are distributed by the Physical Oceanography Distributed Active Archive Center (PODAAC) (NASA Aquarius project 2017; Meissner et al. 2018). There are no finer spatial resolution products available due to its sparser space–time sampling. Its time range is 1 January 2012 to 30 April 2015. The SMAP data are obtained from the SMAP SSS L3 running 8-day V3.0 products at a spatial resolution of 70 km, which are resampled onto a 0.25° × 0.25° by Backus-Gilbert type optimum interpolation (OI) (Meissner et al. 2019). Compared to the previous SMAP product with spatial resolution of 40 km, this 70 km product is recommended to be used for oceanographic applications (Remote Sensing Systems 2018). Besides, the geophysical model function (GMF) of SMAP is same with the Aquarius (Meissner et al. 2018). The time range of this product is 1 April 2015 to 31 December 2017.

To compare the scales from model products with satellite SSS products, our analyses are also applied to two model output, Hybrid Coordinate Ocean Model (HYCOM) and the OGCM For the Earth Simulator (OFES). HYCOM is the popular global ocean circulation model in recent years. Its vertical grids adopt hybrid coordinate, which is isopycnal in the open and stratified ocean, but becomes to a terrain-following coordinate in shallow coastal regions, and to z-level coordinates in the mixed layer or unstratified seas (Chassignet et al. 2007), so it can represent the upper ocean physics better. In this study we used HYCOM global daily GOFS 3.1 reanalysis with 1/12 degree. The daily HYCOM SSS data were resampled every 7 days and interpolated into the same spatial resolutions as the satellite SSS products (0.25° × 0.25°). The OGCM For the Earth Simulator (OFES) is one of the highest resolution global ocean circulation models developed by the Japan Agency for Marine-Earth Science and Technology (JAMSTEC) (Masumoto et al. 2004). This model is based on MOM-3.0. The OFES global 3-day product with 0.1 degree is used in this study. Similar with the HYCOM, the 3-day OFES data were interpolated into 0.25° × 0.25° and resampled every 9 days. The time range of these two model products is 1 January 2011 to 31

December 2017. The sources of all datasets mentioned in this section can be seen in acknowledgements.

The methods for calculating spatial scales are various. Some computed the temporal cross correlation between the target grid point and its neighbors and fitted Gaussian function to it. The scales are determined by the e-folding distances of Gaussian function (Kuragano and Kamachi, 2000; Delcroix et al. 2005). Bingham and Lee (2017) followed the method of Kuragano and Kamachi (2000)**, but the temporal cross correlation didn't fit with a Gaussian function. Tzortzi et al (2016) computed the spatial scales by defining the spatial feature with correlation coefficient $r \geq 1/e$ extending from the target grid to the west, east, north and south directions, respectively. The method of Tzortzi et al (2016) is used in this paper. We firstly calculate the correlation coefficient between time series at each two grid points. The length of SSS spatial scales in four directions (north, south, east and west) are defined as the distance from target grid point to its neighbors when the correlation coefficient first falls below the e-folding threshold. Given the symmetry of the scales in N–S and W–E directions, the zonal and meridional decorrelation scales are determined by averaging the W–E and N–S scales, respectively. As for calculating temporal decorrelation scales, most methods depend on the autocorrelation functions and the temporal decorrelation scales are calculated by the temporal lags of the e-folding decrease or the first zero crossing of the SSS autocorrelation functions (Bingham and Lee 2017). The threshold of e-folding is used in this paper. All time series of SSS filed were detrended before calculating the decorrelation scales.

The salinity budget equation can be expressed as (Feng et al. 1998)

$$\frac{\partial S}{\partial t} = -(u\frac{\partial S}{\partial x} + v\frac{\partial S}{\partial y}) - w_e\frac{S - S_{-h}}{h} - \frac{S(P-E)}{h} + \varepsilon,$$

where S is the sea surface salinity; u and v are the zonal and meridional velocities, respectively; P and E are the precipitation and evaporation rates, and h is the depth of the mixed layer the S_{-h} is the salinity at the bottom of the mixed layer. w_e is the entrainment velocity, $w_e = \frac{dh}{dt} + w_{-h}$,where w_{-h} is the vertical velocity at the bottom of the mixed layer, $w_{-h} = h\left(\frac{\partial u}{\partial x} + \frac{\partial v}{\partial y}\right)$. The left term $\frac{\partial S}{\partial t}$ is the salinity tendency (S_tend), the first term on the right $u\frac{\partial S}{\partial x}$ is the zonal transport term (S_advx), the second term $v\frac{\partial S}{\partial y}$ is the meridional transport term (S_advy), the third term $w_e\frac{S-S_{-h}}{h}$ is the vertical transport term (S_advz), and the fourth term $\frac{S(P-E)}{h}$ is the freshwater flux term (FWF), ε is the error term. Here the CATDS/CEC-OS SMOS Level 4 is used. This product has a spatial resolution of 0.5° and a temporal resolution of 7 days. It also includes key variables to analyze the salinity budget in the upper ocean mixed layer, containing global surface current products from Ocean Surface Current Analyses Realtime (OSCAR), Evaporation from the Objectively Analyzed Air-sea Fluxes (OAFlux) project, Precipitation from CPC MORPHing technique (CMORPH), Mixed Layer Depth from the International Pacific Research Center/Asia–Pacific Data-Research Center (IPRC/APDRC). These fields are averaged in time or interpolated over the week of the SMOS CATDS SSS and gridded at the same spatial resolution. The detail information can be found in the CATDS L4 product data report (CATDS-CECOS Team 2015).

3 Results

3.1 Spatial and temporal scales of the SSS variability

The zonal scales of the SSS field in the tropical Indian Ocean for all six products are shown in Fig. 1. In general, all datasets show similar and coherent spatial decorrelation scale fields. The largest SSS spatial scales for the all datasets are in one noticeable band centred at 8° S (Area1: the central of equatorial Indian Ocean), all with zonal length scales that exceed 2000 km, except for the SMOS Catds data, which has shorter zonal scales not exceeding 1800 km and covers a smaller area. Zonal decorrelation length scales of the magnitude of 1000–1200 km are detected in the centre of the southern Arabian sea (0° N–12° N) (Area 2) in all products. For OFES and HYCOM, large zonal spatial scales dominate most of the North Mozambique channel between 12° S–18° S, in contrast to other satellite products.

For the meridional spatial decorrelation scales (Fig. 2), there are two noticeable areas with large meridional lengths observed in all products. One is located in the south of the Equator with meridional length scale of up to 500–700 km and the other is in the Arabian sea with meridional length scale up to 600–800 km. Meridional decorrelation scales of Aquarius and SMAP in the eastern Arabian Sea are similar and larger than those of the two products of SMOS satellites. Meridional decorrelation length scales on the order of 400–600 km are also observed in the southern of the China South Sea (~ 6° N–15° N, 110° E–120° E). In contrast with other satellite products, OFES and HYCOM show large meridional spatial scales in the North Mozambique channel between 4° S and 24° S. Meanwhile, meridional decorrelation lengths of the SSS field from the model outputs are larger than those obtained from satellite data and cover wider areas. In general, the meridional spatial decorrelation scales are significantly smaller than the zonal scales.

As shown in the ratio of the zonal to meridional length scales of the SSS field (Fig. 3), the spatial decorrelation scales of the tropical Indian Ocean have strong anisotropy. The zonal length scales are larger than the meridional length scales in the central tropical Indian Ocean (12° S–12° N)

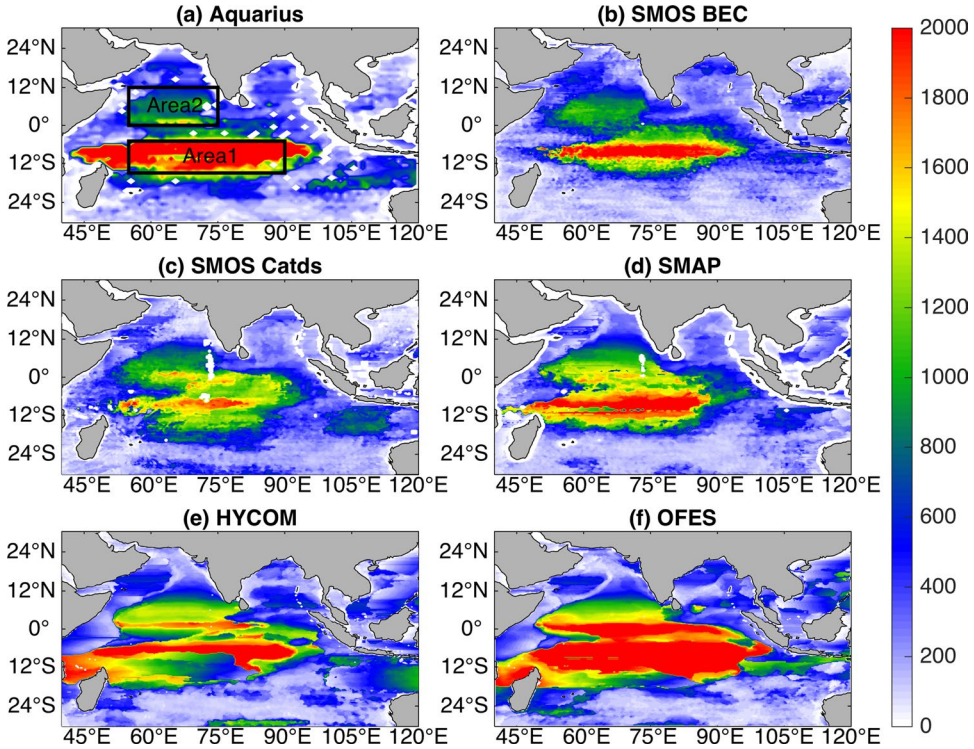

Fig. 1 Zonal decorrelation scales of SSS field in the tropical Indian Ocean calculated from **a** Aquarius, **b** SMOS BEC, **c** SMOS Catds, **d** SMAP, **e** HYCOM, **f** OFES products. The black square marks the location of the central of equatorial Indian Ocean (Area1, 5° S–15° S, 55° E–90° E) and southern region of the Arabian Sea (Area2, 0° N–12° N, 55° E–75° E).The unit is km

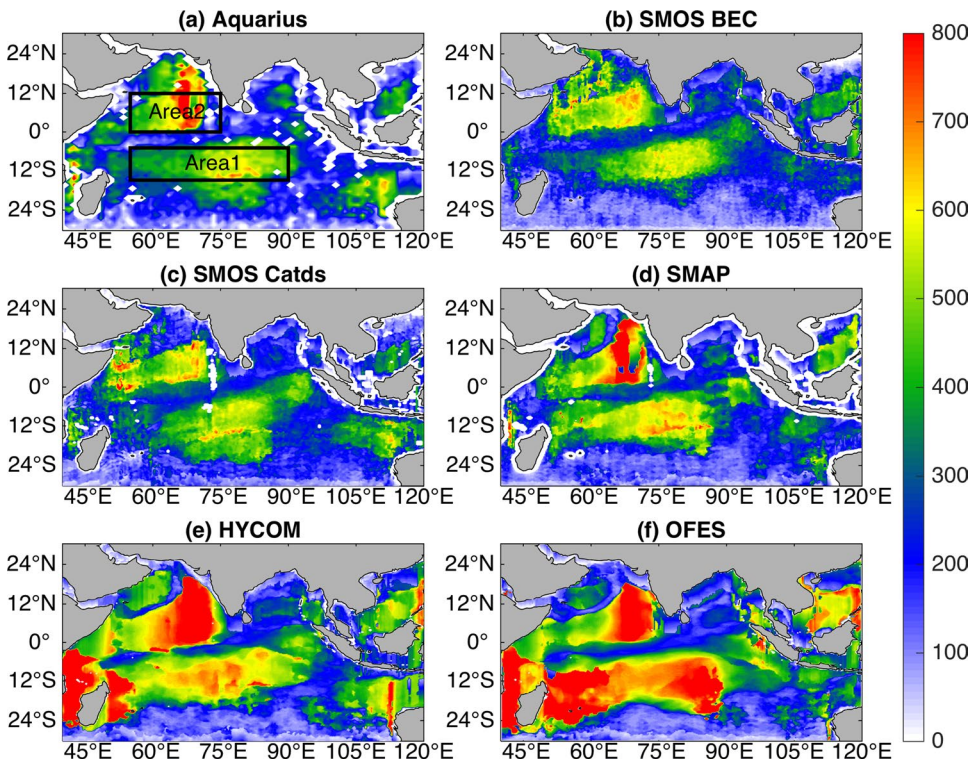

Fig. 2 Meridional decorrelation scales of the SSS field in the tropical Indian Ocean calculated from **a** Aquarius, **b** SMOS BEC, **c** SMOS Catds, **d** SMAP, **e** HYCOM, **f** OFES products. The unit is km

with the maximum ratio up to 6. The ratio decreases from the south of the Equator area towards the tropics, reaching a factor of decimal value along most coasts, which suggests that the zonal scales are smaller than the meridional length scales, especially in the Mozambique Channel (~ 12° S–24° S, 40° E–45° E) and northeastern Arabian sea.

The zonal averages of zonal and meridional decorrelation scales are shown in Fig. 4. Despite the differences in

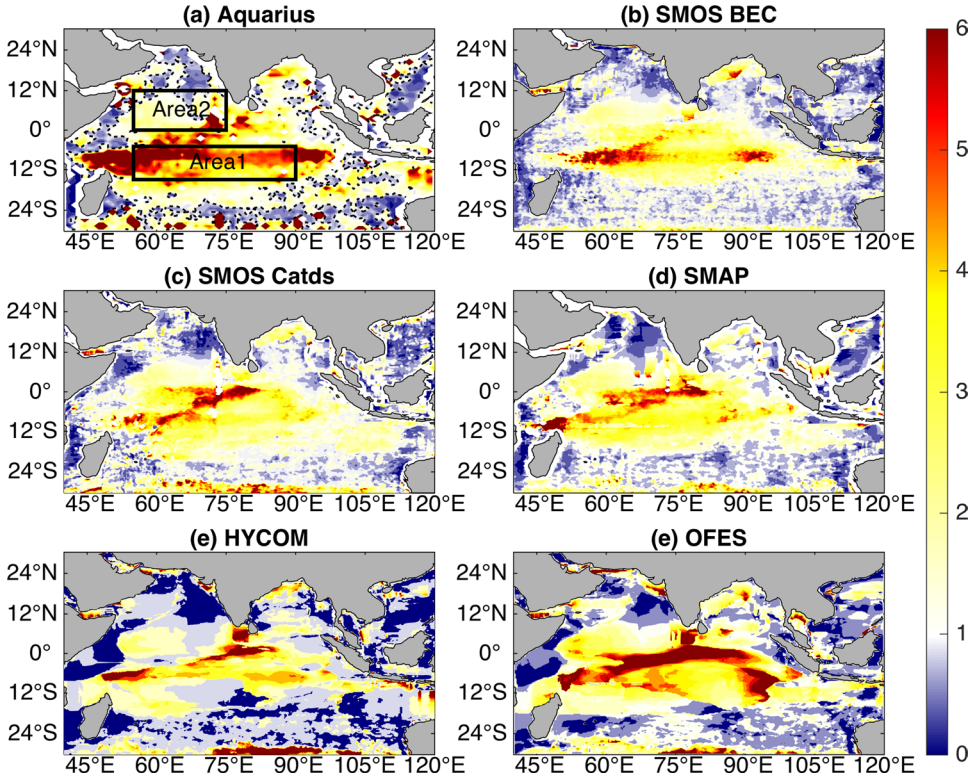

Fig. 3 Ratio of zonal to meridional decorrelation scales of SSS field in the tropical Indian Ocean calculated from **a** Aquarius, **b** SMOS BEC, **c** SMOS Catds, **d** SMAP, **e** HYCOM, **f** OFES products

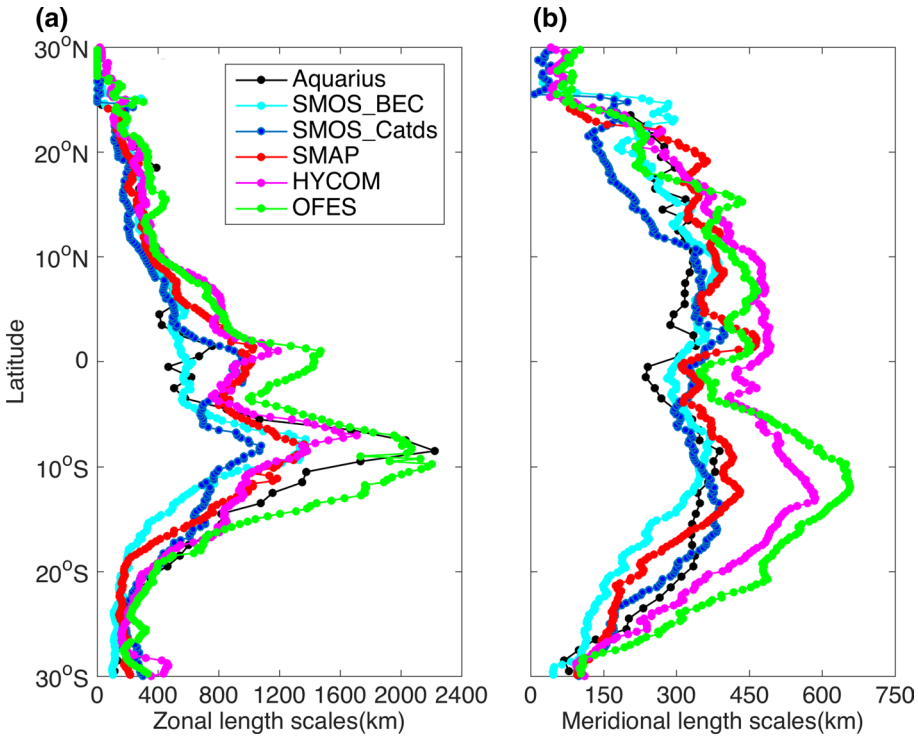

Fig. 4 Zonal averages of (**a**) zonal and (**b**) meridional decorrelation scales of SSS field in the tropical Indian Ocean calculated from different SSS products as indicated by the legend in the panel (**a**)

magnitude, the six products show good consistency. For zonal averages of zonal decorrelation scales, all products except for SMOS BEC suggest a double-peak centred around 5°S (Fig. 4a). It is possible that the less dynamic conditions in the southern equatorial Indian Ocean and the southeastern Arabian Sea (0° N–12° N) may lead to coherent SSS variations over long spatial scales. In addition, all products show good agreement on the short zonal spatial

lengths (< 400 km) in 24° S–30° S and 10° N–30° N regions. Meanwhile, larger meridional spatial lengths are observed for all products around 8° S–15° S (Fig. 4b), especially in the HYCOM and OFES data.

Compared with earlies studies, the spatial scales calculated from satellite data in this study are consistent with those obtained from in situ measurements (Delcroix et al. 2005), with zonal scales on the order of 300–700 km in IX10 track from the Malacca Strait to the Gulf of Aden (Delcroix et al. 2005, Fig. 12), and meridional scales of the order of 200–500 km in IX03 track from La Reunion to the Gulf of Aden (Delcroix et al. 2005; Fig. 8). This indicates that the interpolation radii of the satellite products (0.25°–1°) resolves the short spatial variability in SSS agreement with in situ measurements. In addition, the pattern of spatial scales is consistent with Bingham and Lee (2017; Fig. 7a), although there are differences in spatial scale estimation methods and the SSS data.

As for the temporal scales, all products have three distinct areas of longer persistence in time relative to other regions (Fig. 5). One is observed in the southeast of the Arabian Sea (0–12° N) and another is located in the central of the southern equatorial Indian Ocean (60° E–90° E, 5° S–15° S), both of the time scale is longer than 40 days. The third is located in the northern Bay of Bengal and has temporal scales of approximately 50–60 days. The pattern of longer temporal scales shows great consistency with the larger seasonal amplitude of SSS calculated by Bingham et al. (2012; Fig. 3), which indicates that the temporal scale in these areas (~ 50–70 days) corresponds to a predominance of seasonal variability. Two SMOS products place a very long-lived feature (> 100 days) in the Gulf of Oman. Similarly, HYCOM also has such a feature in the northern Persian Gulf.

The temporal scales of the SSS field for all products are similar with respect to changing latitude (Fig. 6). All products indicate double-peaks at 8° S and 8° N respectively. The

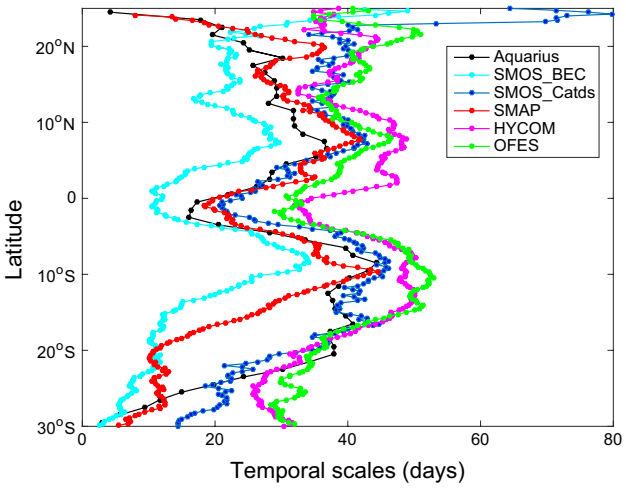

Fig. 6 Zonal averages of temporal decorrelation scales of SSS field in the tropical Indian Ocean calculated from Aquarius, SMOS BEC, SMOS Catds, SMAP, HYCOM and OFES products

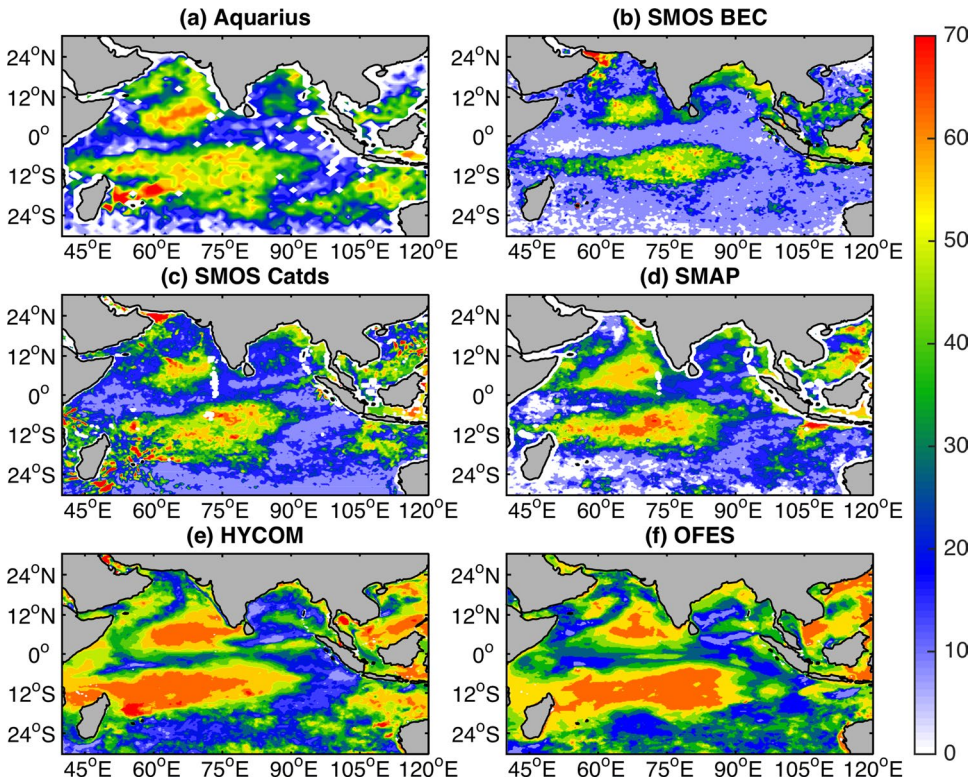

Fig. 5 Temporal decorrelation scales of SSS field in the tropical Indian Ocean calculated from **a** Aquarius, **b** SMOS BEC, **c** SMOS Catds, **d** SMAP, **e** HYCOM, **f** OFES products. The unit is days

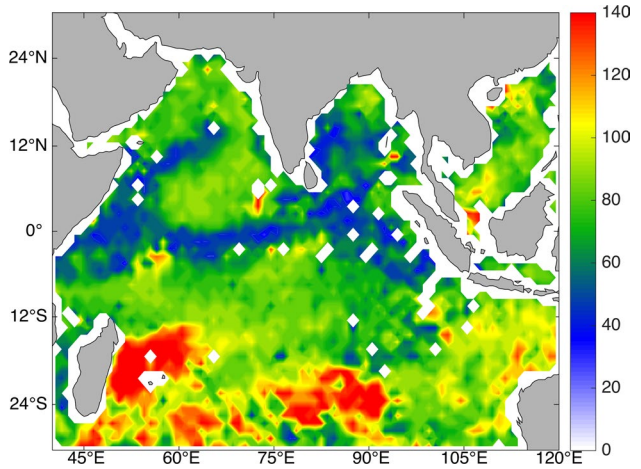

Fig. 7 Temporal decorrelation scales of the SSS field in the tropical Indian Ocean calculated from Aquarius using the same method of Bingham and Lee (2017). The unit is days

data from the two models have generally longer temporal scales than the satellites data except for northward of 22° N. In addition, SMOS BEC and SMOS Catds show longer scales than other products in the band 25–30° N, which can be traced back to longer decorrelation time scales in the gulf of Oman from SMOS BEC and SMOS Catds data. Moreover, the temporal decorrelation scales are smaller than those in Bingham and Lee (2017). This may be due to the differences in the method of calculating decorrelation scale. The first zero crossing of the autocorrelation function (ACF) is chosen as the time scale of SSS in Bingham and Lee (2017), compared with the e-folding time in this study. To compare with the result of Bingham and Lee (2017), the temporal decorrelation scales of SSS field in the tropical Indian Ocean were calculated using the same method of Bingham and Lee (2017) (Fig. 7). The SSS dataset was obtained from Aquarius product, which is similar with the data of Bingham and Lee (2017) (Aquarius Version-4.0 products). When adopting the first zero crossing of the autocorrelation function (ACF) as the time scale, the pattern of temporal scales is in agreement with Bingham and Lee (2017, Fig. 3). The dominant time scales are both around 90 days and areas of longer time scales can be both observed in the southern tropical Indian Ocean near 25° S.

3.2 Salinity budget analysis

The decorrelation scales of SSS in different regions reflect the size of consistent SSS variability in that region. To explain the physical interpretation of SSS variability's scale, the salinity budget equation is used to analyse the effects of different terms (advection term, vertical transport term and freshwater flux term). Figure 8 shows the seasonal variation of regionally averaged salt budget in the central of equatorial Indian Ocean (Area1) and the southern region of the Arabian Sea (Area2), where the large spatial scales with strong anisotropy can be observed in all products (Figs. 1, 2, 3). The different SSS datasets were used for salinity budget analysis in the Area1 and Area 2. A comparison with results

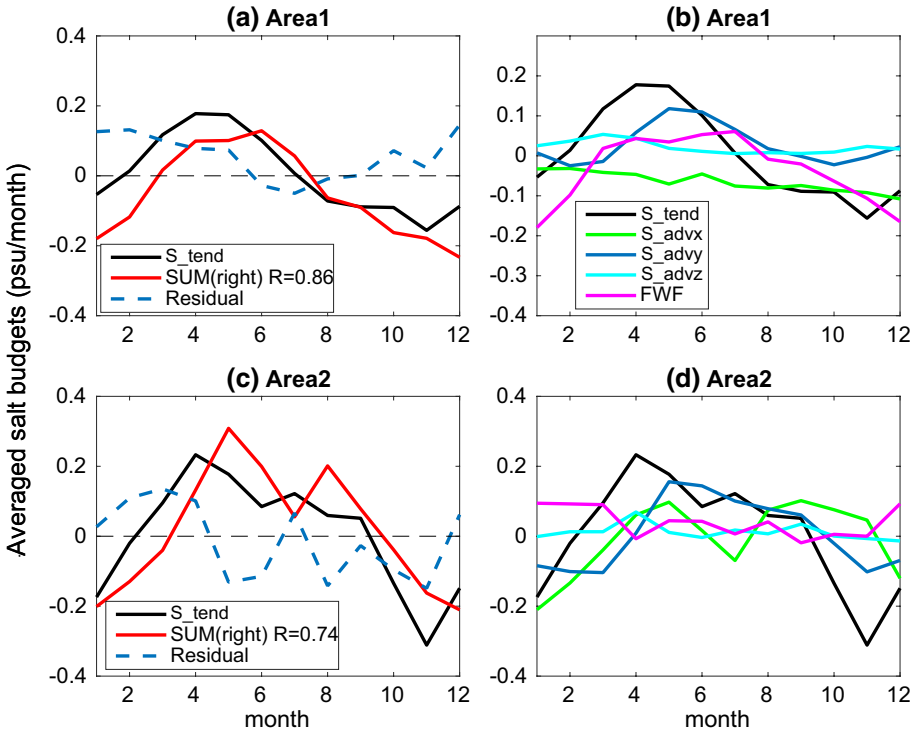

Fig. 8 Seasonal variation of regionally averaged salt budgets, **a**, **b**Area1: central of Equatorial Indian Ocean (5° S–15° S, 60°–80° E), **c**, **d** Area 2: southern region of the Arabian Sea (0°–12° N, 55°E–75° E). SUM (right) represents the sum of the terms on the right side of the salinity budget equation, Residual is the residual term

using the different data sets reveals the averaged SSS tendency from different SSS datasets are in good consistency (not shown). So different SSS datasets have little difference in salinity budget analysis and do not affect the final results.

The SSS tendency in the two regions is consistent with the sum of the terms on the right side of the equation (Fig. 8 a, c). The correlation coefficients are 0.86 and 0.74, respectively. The residual term of Area2 is larger than Area1, but most of them are less than 0.1psu/month. The main reasons for the residual term include the lower-order budget equation used in this paper that cannot represent all the processes that cause SSS variability (such as horizontal mixing and shear instabilities) and the uncertainties in satellite-derived data. The existence of the above errors will not affect the final conclusion. For the central Indian Ocean (Area1), the salinity changes positively from February to July. The meridional transport and freshwater flux terms have a significant effect on the increase in salinity (Fig. 8b). From August to January of the following year, the freshwater flux term is basically consistent with the variation in SSS, which is the main reason for the decrease in SSS. The effect of zonal transport is relatively small (~0.05 psu/month). Meanwhile, The SSS tendency term is positive in the southern region of Arabian Sea (Area2) from March to September (Fig. 8d). During this period, meridional transport is basically consistent with the SSS tendency. From October to February of the second year, SSS tendency term show a negative change. The zonal transport and meridional transport play a major role on the decreasing SSS. The effect of fresh water flux is small during the whole year.

To calculate the relative importance of each term, covariance analysis is performed by pairing each process term with $\frac{\partial S}{\partial t}$ (Yu 2011). The covariance of $\frac{\partial S}{\partial t}$ with a particular process χ_i, is denoted as $\left\langle \chi_i, {}^{\partial S}/_{\partial t} \right\rangle$, and normalization by dividing the sum of the covariance of each process with $\frac{\partial S}{\partial t}$ can be expressed as $\frac{\left|\left\langle \chi_i, {}^{\partial S}/_{\partial t} \right\rangle\right|}{\sqrt{\sum_{i=1}^{4}\left|\left\langle \chi_i, {}^{\partial S}/_{\partial t} \right\rangle\right|}}$, which is defined as the relative importance of the particular process χ_i. Partition of the four leading processes to seasonal variability of $\partial S/\partial t$ is shown in Fig. 9. For the central Indian Ocean (Area 1), the E-P forcing is the first dominant terms, accounting for 51.7% of seasonal variance of the SSS tendency. The meridional transport is of secondary importance and contributes ~30% to $\partial S/\partial t$. By comparison, the other two processes contribute little to the SSS tendency. Meanwhile, the sea surface salinity variation in the southern region of the Arabian Sea are mainly caused by meridional and zonal advection, and their relative importance are 50% and 30%, respectively. Furthermore, the horizontal advection terms were separated into geostrophic (S_adv_Geo) and Ekman component (S_adv_Ekman) and the relative importance of each term was

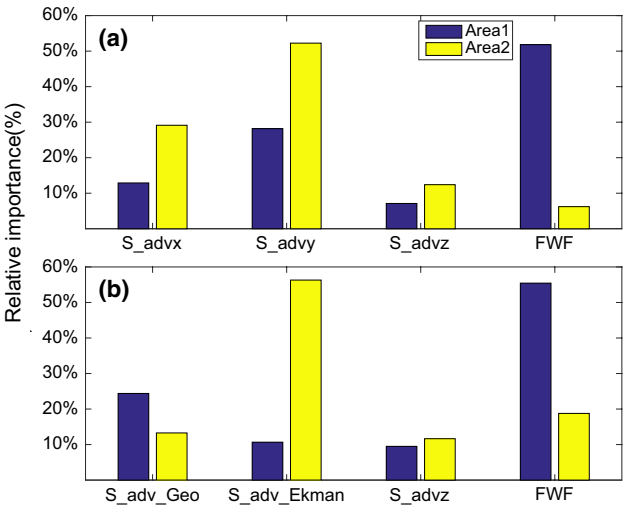

Fig. 9 Relative importance of each contributing process to SSS tendency ($\partial S/\partial t$) in the Area1: central of Equatorial Indian Ocean and Area 2: southern region of the Arabian Sea

calculated (Fig. 9b). For the southern region of the Arabian Sea (Area 2), the Ekman component is more important than the geostrophic component, with the former accounting for 56.3% of seasonal variance of the SSS tendency and the latter 13.2%. In general, surface freshwater fluxes control the seasonal SSS variability on the central of Equatorial Indian Ocean (Area1) (Yu 2011) and the SSS changes in Area2 are mainly driven by the horizontal advection (Rao 2003; Köhler et al. 2018).

The spatial scales of key variables in the salinity budget equation [zonal velocities U, meridional velocities V and freshwater flux (E–P)] are shown in Fig. 10. For Area 1, the zonal and meridional scales of freshwater flux are more consistent with that of SSS. For example, both 12° S latitude bands on the zonal scale of freshwater flux have large value zones, while ocean surface currents (U and V) have little effect. For Area 2, the meridional scales of V coincide with the meridional scale of SSS and there are large scales in the southeast side of the Arabian Sea. The zonal and meridional scale of U coincides with SSS on the southern side of the Arabian Sea. To sum up, the decorrelation scale of SSS in Area 1 is mainly caused by freshwater flux, and the decorrelation scale of SSS in Area 2 mainly results from ocean salinity advection.

4 Conclusions and discussion

Spatial and temporal decorrelation scales of the SSS field were estimated for the first time from long time series of satellite SSS products and two model outputs in the tropical Indian Ocean.

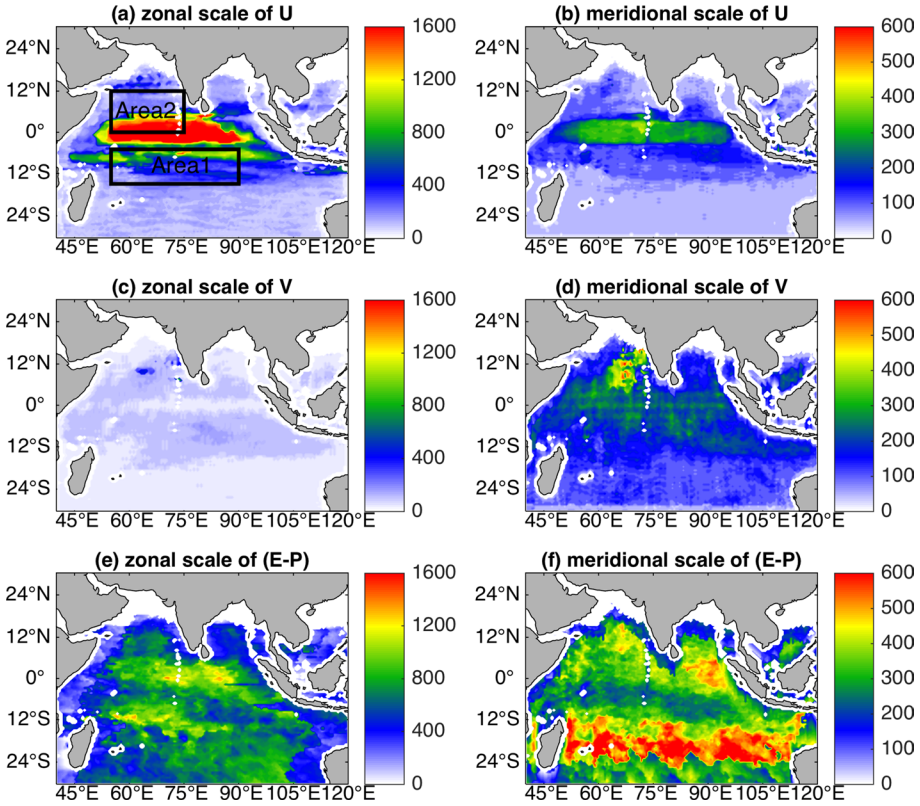

Fig. 10 The spatial scales of key variables in the salinity budget equation over the Tropical Indian Ocean, (**a**, **b**) U (zonal velocities), (**c**, **d**) V (meridional velocities), (**e**, **f**) E-P (evaporation minus precipitation)

Firstly, there are some differences in the decorrelation scales of different satellite products and the results from the two models. For SSS satellite products, it is expected that the procedures and algorithms to produce gridded L3 data from along track-data and L2 data critically affect the results. In addition, differences in temporal and spatial intervals among satellites and the interpolation radii used for the production of SSS products may also contribute to the differences of SSS variability. For example, the zonal spatial scales of Aquarius are longer than other products. It may be caused by the interpolation radii used for the production of the products. The spatial resolution of Aquarius (1°) is lower than that of the other satellite products (0.25°). To verify the effect of interpolation radius on the estimation of decorrelation scales, the SMOS Catds data with different spatial resolutions (1°, 0.5° and 0.25°) are used to calculate the decorrelation scales. Figure 11 shows the information of the of SSS fields in the form of zonal averages from the SMOS Catds data with different spatial resolution and from Aquarius. The change in decorrelation scales with latitude for the four products is similar. The magnitude of spatial scales of SMOS Catds increases as the spatial resolution decreases (from 0.25° to 1°). In addition, the spatial scales of Aquarius are still larger than those of SMOS Catds (1°), despite the same resolution, which may result from the spatial resolution of the two satellite missions. The satellite L2 data are sampled with footprints of approximately 40 km for SMOS and approximately 100–150 km for Aquarius. The wider footprints of the Aquarius data may lead to coherent SSS variations over long spatial scales.

In addition, the optimal interpolation (OI) method already imposes its own spatial scales on the data product. The SMAP product used in this paper uses a circle with a diameter of 70 km as the target cell of the OI. Compared with the previous 40-km resolution product, this 70-km product is smoother on the spatial structures and the random noise is reduced by approximately 60% (Meissner et al. 2019; Remote Sensing Systems 2018). A larger target cell of the OI increases the spatial decorrelation scales. Therefore, the spatial length of SMAP SSS data at a spatial resolution of 70 km are larger than that of the 40-km SMAP product (Fig. 12).

For model data, Tzortzi et al (2016) used satellite SSS data from SMOS and Aquarius to estimate the decorrelation length of SSS in the tropical Atlantic Ocean and found that the decorrelation scales were larger than those from an eddy-resolving general circulation model with 4-km spatial resolution and a daily temporal resolution (Martins et al. 2015). Tzortzi (2016) hypothesized that this may be due to the fine temporal and spatial resolution of the model data (daily, 4 km), which can capture small scale spatial distribution and higher-frequency temporal variability of the SSS field. In this study, we verified this hypothesis by comparing the results from ocean model products (HYCOM and

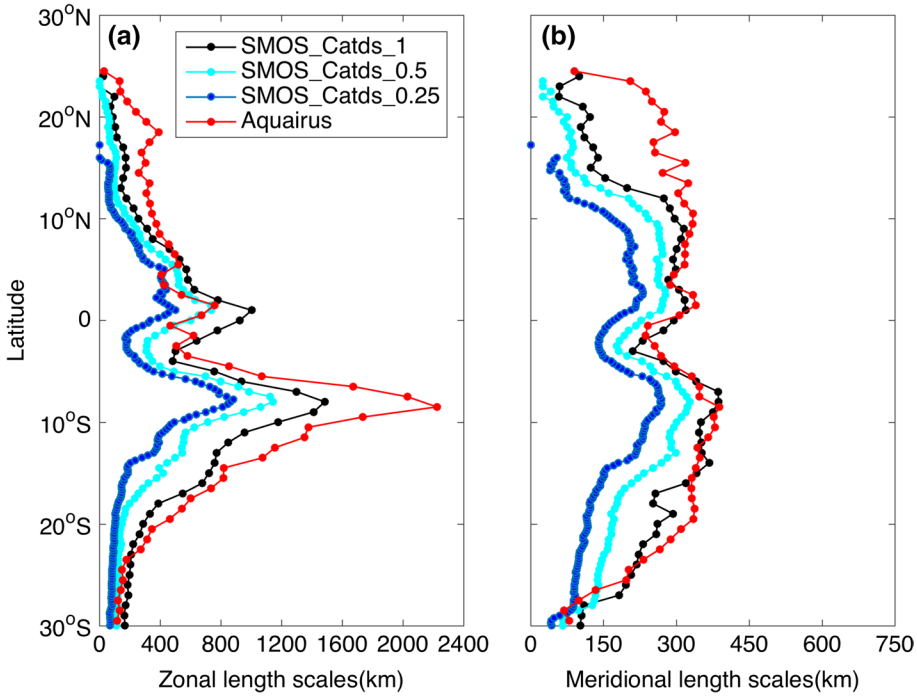

Fig. 11 Zonal averages of (**a**) zonal and (**b**) meridional decorrelation scales of SSS field in the tropical Indian Ocean calculated from different SSS products as indicated by the legend in the panel (**a**)

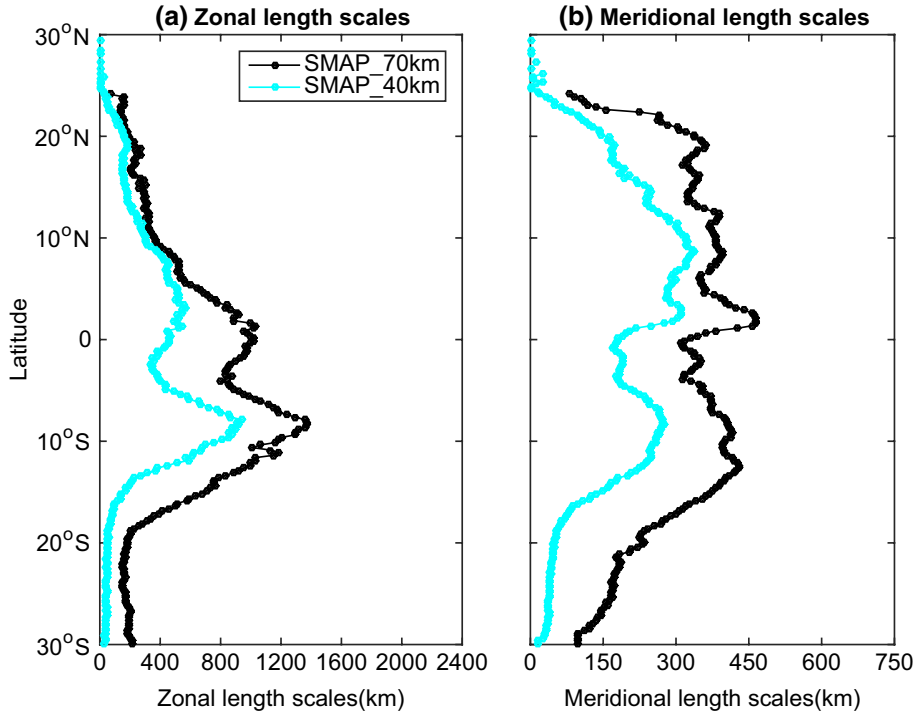

Fig. 12 Zonal averages of (**a**) zonal and (**b**) meridional decorrelation scales of SSS field in the tropical Indian Ocean calculated from the 40-km SMAP and 70-km SMAP product

OFES) applying the same resolution as the satellite SSS products and the same scales estimation methods. In general, the decorrelation scales of SSS field from the model output are larger than those obtained from the satellite data (Figs. 4, 6). This may be due to the fact that the SSS data from the model are calculated by the physical equations and have more constraints, such as the relaxation of the model to the climatology, making SSS changes more homogeneous than those from satellite SSS retrieved using brightness temperature.

Despite the difference in the spatial and temporal resolution and data periods of the six products, there is generally good agreement in the spatial and temporal scales of the SSS field, which indicates that these factors have a limited

effect on the scales of SSS variability. For example, the large spatial scale with strong anisotropy in the central equatorial Indian Ocean and the southern region of the Arabian Sea (0° N–12° N) can be observed in all products. The salinity budget analysis shows that the processes FWF and salinity advection are the dominant processes in these two areas, respectively. However, it should be noted that the SSS decorrelation scales are dominated by the joint effect of several terms instead of one single term.

It is worth noting that very short spatial and temporal scales in the SSS field cannot be resolved by limiting the interpolation radii used for the production of products in this study (0.25°–1.0°; 7–9 days), such as in the southern tropical Indian Ocean (25° S–30° S). Our results are beneficial for understanding the controlling mechanisms of SSS variability. Future studies may include the exploration of the relationship between spatial and temporal scales of SSS variability with atmospheric forcing (such as Indian monsoon) and oceanic processes using satellite data, in situ observations and model outputs, which will further improve the knowledge of the variability and controlling mechanisms of SSS.

Acknowledgements This work was supported by National Natural Science Foundation of China (41976188 and 41706021). The SMOS L3 BEC products are distributed by BEC from sftp://becftp.icm.csic.es. The SMOS L3_DEBIAS_LOCEAN_v2 Sea Surface Salinity maps have been produced by LOCEAN/IPSL (UMR CNRS/UPMC/IRD/MNHN) laboratory and ACRI-st company that participate to the Ocean Salinity Expertise Center (CECOS) of Centre Aval de Traitement des Donnees SMOS (CATDS), which can be downloaded from ftp://ext-catds-cecos-locean:catds2010@ftp.ifremer.fr/. Aquarius data are provided by NASA's Physical Oceanography Distributed Active Archive Center (PO.DAAC) (https://doi.org/10.5067/AQR50-3Y7CE). SMAP data are produced by Remote Sensing Systems and sponsored by the NASA Ocean Salinity Science Team. They are available at https://dx.doi.org/10.5067/SMP40-3SPCS. The HYCOM data are available at https://apdrc.soest.hawaii.edu:80/dods/ public_ofes/HYCOM/GLBv0.08/daily_snapshot. The OFES simulation was conducted on the Earth Simulator under the support of JAMSTEC, which are available at https://apdrc.soest.hawaii.edu:80/dods/public_ofes/ OfES/ncep_0.1_global _3day/salt. The altimeter products (SSH data) were produced by SSALTO/ DUACS and distributed by AVISO with support from CNES (https://www.aviso.oceanobs.com/duacs/).

References

Ballabrera-Poy J, Murtugudde R, Busalacchi AJ (2002) On the potential impact of sea surface salinity observations on ENSO predictions. J Geophys Res. https://doi.org/10.1029/2001JC000834

Bao S, Zhang R, Wang H, Yan H, Yu Y, Chen J (2019) Salinity profile estimation in the Pacific Ocean from satellite surface salinity observations. J Atmos Ocean Technol 36(1):53–68. https://doi.org/10.1175/JTECH-D-17-0226.1

Belward A, Bourassa MA, Dowell M, Briggs S (2016) The Global Observing System for climate: implementation needs GCOS-200, https://unfccc.int/files/science/workstreams/systematic_observation/application/pdf/gcos_ip_10oct2016.pdf

Bingham FM, Lee T (2017) Space and time scales of sea surface salinity and freshwater forcing variability in the global ocean (60S–60N). J Geophys Res. https://doi.org/10.1002/2013JC009262

Bingham FM, Foltz GR, McPhaden MJ (2012) Characteristics of the seasonal cycle of surface layer salinity in the global ocean. Ocean Sci 8(5):915–929. https://doi.org/10.5194/os-8-915-2012

Boutin J, Vergely JL, Marchand S, Amico FD, Hasson A, Kolodziejczyk N et al (2018) New SMOS Sea Surface Salinity with reduced systematic errors and improved variability. Remote Sens Environ 214:115–134. https://doi.org/10.1016/j.rse.2018.05.022

CATDS-CECOS Team (2015) SMOS Level 4 Thematic SSS Research products-Product User Manual. ftp://ext-catds-cecos-locean:catds2010@ftp.ifremer.fr/Ocean_products/documentation/CATDS-CECOS_SMOS_level4Products_UserDocument_V1.pdf.

Chassignet EP, Hurlburt HE, Smedstad OM, Halliwell GR, Hogan PJ, Wallcraft AJ et al (2007) The HYCOM (HYbrid Coordinate Ocean Model) data assimilative system. J Mar Syst 65(1):60–83

de Boyer MC, Mignot J, Lazar A, Cravatte S (2007) Control of salinity on the mixed layer depth in the world ocean: 1. General description. J Geophys Res 112(6):1–12. https://doi.org/10.1029/2006JC003953

Delcroix T, McPhaden MJ, Dessier A, Gouriou Y (2005) Time and space scales for sea surface salinity in the tropical oceans. Deep-Sea Res Part I 52(5):787–813. https://doi.org/10.1016/j.dsr.2004.11.012

Du Y, Zhang Y (2015) Satellite and Argo observed surface salinity variations in the tropical Indian Ocean and their association with the Indian ocean dipole mode. J Clim 28:695–713. https://doi.org/10.1175/JCLI-D-14-00435.1

Durack PJ, Matear RJ (2012) Ocean salinities reveal strong global water cycle intensification during 1950 to 2000. Science 336(6080):455–458

Durand F, Alory G, Dussin R, Reul N (2013) SMOS reveals the signature of Indian Ocean Dipole events. Ocean Dyn 63:1203–1212. https://doi.org/10.1007/s10236-013-0660-y

Felton CS, Subrahmanyam B, Murty VSN, Shriver JF (2015) Estimation of the barrier layer thickness in the Indian Ocean using Aquarius Salinity. J Geophys Res Oceans 119(7):4200–4213

Feng M, Hacker P, Lukas R (1998) Upper ocean heat and salt balances in response to a westerly wind burst in the western equatorial Pacific during TOGA COARE. J Geophys Res Ocean. https://doi.org/10.1029/97jc03286

Fournier S, Lee T, Gierach MM (2016) Seasonal and interannual variations of sea surface salinity associated with the Mississippi River plume observed by SMOS and Aquarius. Remote Sens Environ 180:431–439. https://doi.org/10.1016/j.rse.2016.02.050

Grunseich G, Subrahmanyam B, Murty VSN, Giese BS (2011) Sea surface salinity variability during the Indian Ocean Dipole and ENSO events in the tropical Indian Ocean. J Geophys Res Ocean 116:1–14. https://doi.org/10.1029/2011JC007456

Hasson A, Puy M, Boutin J, Guilyardi E, Morrow R (2018) Northward pathway across the tropical north Pacific Ocean revealed by surface salinity: how do El Niño Anomalies reach Hawaii? J Geophys Res 123(4):2697–2715. https://doi.org/10.1002/2017JC013423

Hosoda K, Kawamura H (2004) Global space-time statistics of sea surface temperature estimated from AMSR-E data. Geophys Res Lett 31(17):1–5. https://doi.org/10.1029/2004GL020317

Jacobs GA, Barron CN, Rhodes RC (2001) Mesoscale characteristics. J Geophys Res Oceans 106(C9):19581–19595

Köhler J, Serra N, Bryan FO et al (2018) Mechanisms of mixed-layer salinity seasonal variability in the Indian Ocean. J Geophys Res Ocean 123:466–496. https://doi.org/10.1002/2017JC013640

Kuragano T, Kamachi M (2000) Global statistical space-time scales of oceanic variability estimated from the TOPEX/POSEIDON altimeter data. J Geophys Res 105(C1):955–974. https://doi.org/10.1029/1999jc900247

Li J, Liang C, Tang Y et al (2016) A new dipole index of the salinity anomalies of the tropical Indian Ocean. Sci Rep. https://doi.org/10.1038/srep24260

Martins MS, Serra N, Stammer D (2015) Spatial and temporal scales of sea surface salinity variability in the Atlantic Ocean. J Geophys Res Oceans 120(6):4306–4323

Masumoto Y, Sasaki H, Kagimoto T, Komori N, Ishida A, Sasai Y et al (2004) A fifty-year eddy-resolving simulation of the world ocean: preliminary outcomes of OFES (OGCM for the Earth Simulator). J Earth Simul 1:35–56

Meissner T, Wentz FJ, Le Vine DM (2018) The salinity retrieval algorithms for the NASA Aquarius version 5 and SMAP version 3 releases. Remote Sens. https://doi.org/10.3390/rs10071121

Meissner T, Wentz FJ, Manaster A, Lindsley R (2019) Remote sensing systems SMAP ocean surface salinities level 3 running 8-day, Version 4.0 validated release. Remote Sens Syst. https://doi.org/10.5067/SMP40-3SPCS

Melnichenko O, Hacker P, Maximenko N, Lagerloef G, Potemra J (2014) Spatial optimal interpolation of aquarius sea surface salinity: algorithms and implementation in the North Atlantic. J Atmos Ocean Technol 31(7):1583–1600. https://doi.org/10.1175/JTECH-D-13-00241.1

Menezes VV, Vianna ML, Phillips HE (2014) Aquarius sea surface salinity in the South Indian Ocean: revealing annual period planetary waves. J Geophys Res. https://doi.org/10.1002/2014JC009935

Meyers G, Phillips H, Smith N, Sprintall J (1991) Space and time scales for optimal interpolation of temperature. Tropical Pacific Ocean. Prog Oceanogr 28:189–218

Momin IM, Mitra AK, Prakash S et al (2015) Variability of sea surface salinity in the tropical Indian Ocean as inferred from Aquarius and in situ data sets. Int J Remote Sens 36:1907–1920. https://doi.org/10.1080/01431161.2015.1030045

Mu Z, Zhang W, Wang P, Wang H, Yang X (2019) Assimilation of SMOS sea surface salinity in the regional ocean model for South China Sea. Remote Sens. https://doi.org/10.3390/rs11080964

NASA Aquarius Project (2017) Aquarius official release level 3 rain-flagged sea surface salinity standard mapped image monthly data V5.0. Ver. 5.0. PO.DAAC, CA, USA. Accessed 03 Mar 2019.

Nyadjro ES, Subrahmanyam B (2016) Spatial and temporal variability of central Indian Ocean salinity fronts observed by SMOS. Remote Sens Environ 180:146–153. https://doi.org/10.1016/j.rse.2016.02.049

Olmedo E, Martínez J, Turiel A, Ballabrera-Poy J, Portabella M (2017) Debiased non-Bayesian retrieval: a novel approach to SMOS sea surface salinity. Remote Sens Environ 193:103–126

Rao RR (2003) Seasonal variability of sea surface salinity and salt budget of the mixed layer of the north Indian Ocean. J Geophys Res 108:3009. https://doi.org/10.1029/2001JC000907

Remote Sensing Systems (2018) New SMAP sea surface salinity (SSS) 70km data. https://smap.jpl.nasa.gov/news/1265/smap-sees-sea-surface-salinity/

Subrahmanyam B, Murty VSN, Heffner DM (2011) Sea surface salinity variability in the tropical Indian Ocean. Remote Sens Environ 115:944–956. https://doi.org/10.1016/j.rse.2010.12.004

Tzortzi E, Srokosz M, Gommenginger C, Josey SA (2016) Spatial and temporal scales of variability in Tropical Atlantic sea surface salinity from the SMOS and Aquarius satellite missions. Remote Sens Environ 180:418–430. https://doi.org/10.1016/j.rse.2016.02.008

Wang H, Zhang R (2012) Freshwater flux product reconstruction based on Argo data and mixed layer model. Acta Phys Sin 61(3):1–6. https://doi.org/10.7498/aps.61.039202

Yan H, Zhang R, Wang G, Wang H, Chen J, Bao S (2019) Improved multifractal fusion method to blend SMOS sea surface salinity based on semiparametric weight function. J Atmos Ocean Technol 36(8):1501–1520. https://doi.org/10.1175/jtech-d-18-0155.1

Yu L (2011) A global relationship between the ocean water cycle and near-surface salinity. J Geophys Res Ocean 116:1–17. https://doi.org/10.1029/2010JC006937

Zhang Y, Du Y, Qu T (2016) A sea surface salinity dipole mode in the tropical Indian Ocean. Clim Dyn 47:2573–2585. https://doi.org/10.1007/s00382-016-2984-z

Zhang Y, Du Y, Feng M (2018) Multiple time scale variability of the sea surface salinity dipole mode in the tropical Indian Ocean. J Clim 31:283–296. https://doi.org/10.1175/JCLI-D-17-0271.1

Zhu J, Huang B, Zhang R-H, Hu Z-Z, Kumar A, Balmaseda M et al (2014) Salinity anomaly as a trigger for ENSO events. Sci Rep 4:6821. https://doi.org/10.1038/srep06821